

evaporation<sup>17</sup>. Taking the mean density and Bond albedo of a typical Vulcanoid to be the same as that of Mercury, we find that objects with radii  $z$  satisfying  $0.1 \leq z \leq 50$  km can evade both drag and evaporation in the Vulcanoid belt. This is one of the most dynamically stable regimes in the entire Solar System. If further searches do not detect any intra-mercurial objects, this is a strong indicator that other processes—such as planetary migrations—may have disrupted the population.

Although there are no known intra-mercurial bodies, we can find candidate objects for the Earth–Mars belt. Suppose we search an asteroidal database<sup>18</sup> for objects with inclinations  $i < 10^\circ$  and eccentricities  $e < 0.2$  between the semimajor axes of Earth and Mars, then we find that there are ten objects. Of these, seven lie within our suggested Earth–Mars belt (1.08–1.28 AU), which is evidence for an enhancement of nearly circular orbits in this region. An even more striking test is to search through the objects between the Earth and Mars for asteroids of low eccentricity and inclination that are not planet-crossing. There are only three such objects (1996 XB27, 1998 HG49 and 1998 KG3) among all the asteroids in this database, and all three lie between 1.08 and 1.28 AU. Most of the  $\sim 50$  asteroids with semimajor axes at present located in our Earth–Mars belt are moving on orbits with large eccentricities and inclinations. They are not dynamically stable, and will evolve on timescales of the order of a few million years. Most of these objects are believed to be asteroids ejected from resonance locations in the main belt, although a handful may even be comets whose surfaces have become denuded of volatiles<sup>19</sup>. However, the seeming enhancement of circular orbits in this region hints at a primordial population whose orbits are very slightly eccentric and slightly inclined. Ejection from the main belt will tend to increase the eccentricity of an asteroid<sup>20</sup>. So the slightly eccentric objects may well be remnant planetesimals, the original denizens of the region before it was colonized by asteroids from the resonance locations in the main belt. □

Received 26 October 1998; accepted 12 March 1999.

1. Kowal, C. T. in *Asteroids* (ed. Gehrels, T.) 436–439 (Univ. Arizona Press, Tucson, 1979).
2. Jewitt, D. & Luu, J. X. Discovery of the candidate Kuiper belt object 1992 QB1. *Nature* **362**, 730–732 (1993).
3. Williams, I. P., O'Cellaigh, D. P., Fitzsimmons, A. & Marsden, B. G. The slow-moving objects 1993 SB and 1993 SC. *Icarus* **116**, 180–185 (1995).
4. Holman, M. J. A possible long-lived belt of objects between Uranus and Neptune. *Nature* **387**, 785–788 (1997).
5. Wisdom, J. & Holman, M. J. Symplectic maps for the n-body problem. *Astron. J.* **102**, 1528–1538 (1991).
6. Saha, P. & Tremaine, S. D. Symplectic integrators for solar system dynamics. *Astron. J.* **104**, 1633–1640 (1992).
7. Saha, P. & Tremaine, S. D. Long term planetary integration with individual time steps. *Astron. J.* **108**, 1962–1969 (1994).
8. Holman, M. J. & Wisdom, J. Dynamical stability in the outer solar system and the delivery of short period comets. *Astron. J.* **105**, 1987–1999 (1993).
9. Danby, J. M. A. *Fundamentals of Celestial Mechanics* (Willmann-Bell, Richmond, 1988).
10. Mikkola, S. & Innanen, K. Solar system chaos and the distribution of asteroid orbits. *Mon. Not. R. Astron. Soc.* **277**, 497–501 (1995).
11. Weidenschilling, S. J. Iron/silicate fractionation and the origin of Mercury. *Icarus* **35**, 99–111 (1978).
12. Leake, M. A., Chapman, C. R., Weidenschilling, S. J., Davis, D. R. & Greenberg, R. The chronology of Mercury's geological and geophysical evolution—The Vulcanoid hypothesis. *Icarus* **71**, 350–375 (1987).
13. Campins, H., Davis, D. R., Weidenschilling, S. J. & Magee, M. in *Completing the Inventory of the Solar System* (eds Rettig, T. W. & Hahn, J. M.) 85–96 (ASP Conf. Proc., Astron. Soc. Pacif., San Francisco, 1996).
14. Dones, L., Levison, H. F. & Duncan, M. in *Completing the Inventory of the Solar System* (eds Rettig, T. W. & Hahn, J. M.) 233–244 (ASP Conf. Proc., Astron. Soc. Pacif., San Francisco, 1996).
15. Weissman, P. R., A'Hearn, M. F., McFadden, L. A. & Rickman, H. in *Asteroids II* (eds Binzel, R. P., Gehrels, T. & Matthews, M. S.) 880–920 (Univ. Arizona Press, Tucson, 1989).
16. Robertson, H. P. Dynamical effects of radiation in the solar system. *Mon. Not. R. Astron. Soc.* **97**, 423–438 (1937).
17. Pettit, E. in *Planets and Satellites* (eds Kuiper, G. P. & Middlehurst, B.) 400–427 (Univ. Chicago Press, 1961).
18. Bowell, E. G. *The Asteroid Orbital Element Database* at ([ftp://ftp.lowell.edu/pub/elg/astorb.html](http://ftp.lowell.edu/pub/elg/astorb.html)).
19. McFadden, L. A., Tholen, D. J. & Veeder, G. J. in *Asteroids II* (eds Binzel, R. P., Gehrels, T. & Matthews, M. S.) 442–467 (Univ. Arizona Press, Tucson, 1989).
20. Gladman, B. et al. Dynamical lifetimes of objects injected into asteroid belt resonances. *Science* **277**, 197–201 (1997).
21. Saha, P., Stadel, J. & Tremaine, S. D. A parallel integration method for solar system dynamics. *Astron. J.* **114**, 409–414 (1997).

**Acknowledgements.** We thank P. Saha and S. Tremaine for suggestions and comments, as well as their advice on computational matters, and J. Chambers, M. Holman and L. Dones for helpful criticism. The Royal Society supported the purchase of dedicated computers, and we also thank the Oxford Supercomputing Centre (OSCAR) for support.

Correspondence and requests for materials should be addressed to N.W.E. (e-mail: [nwe@thphys.ox.ac.uk](mailto:nwe@thphys.ox.ac.uk)).

## Observation of mesoscopic vortex physics using micromechanical oscillators

C. A. Bolle\*, V. Aksyuk\*, F. Pardo\*, P. L. Gammel\*, E. Zeldov‡, E. Bucher\*, R. Boie\*, D. J. Bishop\* & D. R. Nelson†

\* Bell Laboratories, Lucent Technologies, 700 Mountain Avenue, Murray Hill, New Jersey 07974, USA

† Department of Physics, Harvard University, Cambridge, Massachusetts 02138, USA

It has long been known that magnetic fields penetrate type II superconductors in the form of quantized superconducting vortices. Most recent research in this area has, however, focused on the collective properties of large numbers of strongly interacting vortices<sup>1,2</sup>: the study of vortex physics on the mesoscopic scale (a regime in which a small number of vortices are confined in a small volume) has in general been hampered by the lack of suitable experimental probes. Here we use a silicon micromachined mechanical resonator to resolve the dynamics of single vortices in micrometre-sized samples of the superconductor 2H-NbSe<sub>2</sub>. Measurements at and slightly above the lower critical field,  $H_{c1}$  (the field at which magnetic flux first penetrates the superconductor), where only a few vortices are present, reveal a rich spectrum of sharp, irreversible vortex rearrangements. At higher fields, where tens of vortices are present, the sharp features become reversible, suggesting that we are resolving a new regime of vortex dynamics in which the detailed configuration of pinning sites, sample geometry and vortex interactions produce significant changes in the measurable vortex response. This behaviour can be described within the framework of interacting vortex lines in a '1 + 1'-dimensional random potential—an important (but largely untested) theoretical model for disorder-dominated systems<sup>11,12</sup>.

High-Q mechanical oscillators have previously been shown to be powerful probes of condensed matter<sup>3–5</sup>. However, the recent availability of silicon micromechanics has enormously expanded the power of the technique by allowing high Q and also small size. Figure 1 shows a scanning electron micrograph of our micromachine. The mechanical oscillator consists of a plate connected via two serpentine springs to two support structures attached to the substrate. Under the plate are two electrodes on the silicon substrate. The outline of the electrodes is visible on the top plate owing to print-through during the multiple processing steps. In operation, the device is oscillated torsionally about the long axis of the plate. One electrode is used to drive the plate and the other to detect the actual movement. This torsional mode has a resonant frequency of 45 kHz and a Q of 250,000 at low temperatures. The device was built by using a three-layer polysilicon process at the MCNC foundry (<http://www.mcnc.org>).

The inset to Fig. 1 shows an enlargement of the sample used for the studies described here. It is a single crystal of 2H-NbSe<sub>2</sub> with dimensions of  $22 \times 49 \times 1.6 \mu\text{m}^3$ . The sample is from a batch of very-high-quality single crystals with typical critical current densities of  $100 \text{ A cm}^{-2}$  and weak pinning, producing well-ordered flux lattices at low fields as observed with magnetic decoration<sup>6,7</sup>. Other measurements have confirmed the high quality of these crystals<sup>8</sup>. The  $T_c$  of our sample was 7.0 K. The sample was glued onto the oscillator with a microgluing technique that allows us to affix submicrometre-sized particles with precision.

A magnetic field was applied parallel to the face of the crystal and

‡ Permanent address: Department of Condensed Matter Physics, Weizmann Institute of Science, Rehovot 76100, Israel.

perpendicular to its rotation axis. A sample with a magnetic moment  $\mathbf{M}$  in a field  $\mathbf{H}$  exerts an additional torque  $\boldsymbol{\tau} = \mathbf{M} \times \mathbf{H}$  on the oscillator, shifting its resonant frequency. The small size of the oscillator allows us to obtain high resonant frequencies despite the soft spring constants, typically  $\sim 0.5 \times 10^{-9}$  N m.

Figure 2 shows the frequency and amplitude dependence for a standard zero-field-cooled (ZFC)/field-cooled (FC) temperature sweep. We can see that these oscillators have very little temperature-dependent background, as shown by the black lines. After applying a field of 60 Oe at 5 K we observe a frequency shift of roughly 20 Hz and no change in the oscillator's amplitude. This is a clear signature of the Meissner state. The energy cost of screening a magnetic field applied parallel to the face of a thin superconductor is smaller than the cost of screening the same field applied perpendicular to the face of the sample. The resulting variation in the torque with the tilt angle  $d\tau/d\theta$  causes a restoring force that increases the oscillator frequency. The result is an increase in the oscillator frequency with no change in the amplitude (no dissipation). As we warm up the sample (red line) we see a slight decrease in the Meissner restoring force as  $\lambda(T)$  starts to become comparable to the sample thickness.

At  $T \approx 6.1$  K we see a sudden decrease in the oscillator amplitude and a jump in its frequency. These changes are associated with the first flux line penetration and uniquely define the location of the first penetration field  $H_p$  for our sample. We can use the approximation  $H_{c1} \approx H_p$  for the lower critical field because the demagnetizing factor for this field direction is very small. Note the increase in the 'noise' in the data that, as we show below, is the resolution of single-vortex events in the oscillator. As we approach  $T_c$  both the frequency and the amplitude merge into the background. On cooling of the sample (blue line) in the presence of the 60 Oe field, the flux lines nucleate in the superconductor below  $T_c$ , resulting in a frequency shift and a decrease in amplitude (increase in dissipation). Both the frequency shift and the amplitude show a

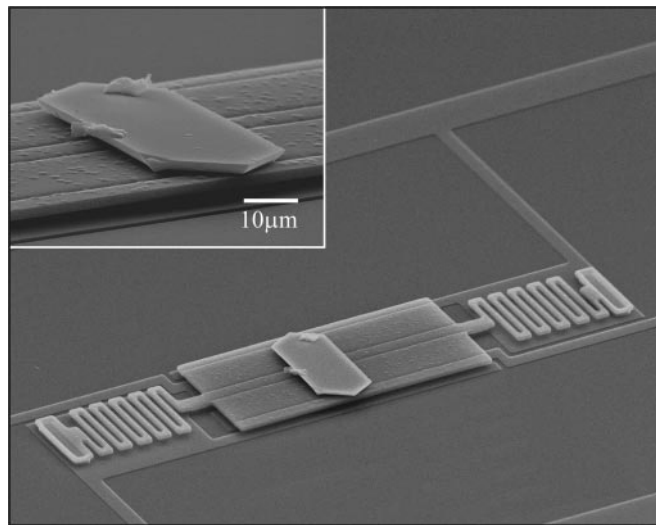


**Figure 1** Scanning electron micrograph of a high-Q mechanical oscillator with a hexagonal single crystal of the traditional superconductor 2H-NbSe<sub>2</sub> mounted on top. The oscillator was manufactured in a three-layer polysilicon process. The paddle of the oscillator, formed from the third layer, is freely suspended by two springs anchored to the substrate at its ends. Two electrodes, formed from the first polysilicon layer and located directly under the paddle, are used to excite it in a torsional resonance mode. The gap between the electrodes and the paddle is fixed by the multilayer process and is 2.75  $\mu\text{m}$ . The sample is mounted and glued to the paddle with the help of a micropipette. The inset shows a detail of the sample. The thickness of the sample is slightly larger than the 1.5- $\mu\text{m}$ -thick paddle.

rich structure close to  $T_c$  that tends to smooth out at lower temperatures. This structure represents the changes in the pinning strength of the vortex ensemble as the number of flux lines changes.

Figure 3a shows a field sweep close to  $T_c$  after a ZFC. The frequency shift in the Meissner state due to the shielding currents up to  $H_{c1} \approx 9$  Oe has the expected  $H^2$  dependence, because  $\mathbf{M} = (-1/4\pi)\mathbf{H}$  and  $\boldsymbol{\tau} = \mathbf{M} \times \mathbf{H}$ . Above  $H_{c1}$  we see a series of peaks in the frequency that we interpret as the signature of the first several flux lines entering the sample. The field scale and the size of the sample are consistent with this interpretation. As we shall argue below, the first flux lines that go into the sample wander significantly away from the field direction to take advantage of the point disorder. As the field increases, more lines enter the sample and these wandering lines start to interact. Figure 3b shows the response at a lower-temperature ZFC field sweep. The Meissner regime is once again quadratic but the penetration of single vortices above  $H_{c1}$  is somewhat different owing to the stronger effects of pinning at lower temperatures. At this temperature, as the individual vortices enter, there are mesas between the jumps. As the field is cycled back and forth a fraction of an oersted, the response in the mesas is reversible but the jumps are not. The reason for the non-monotonic

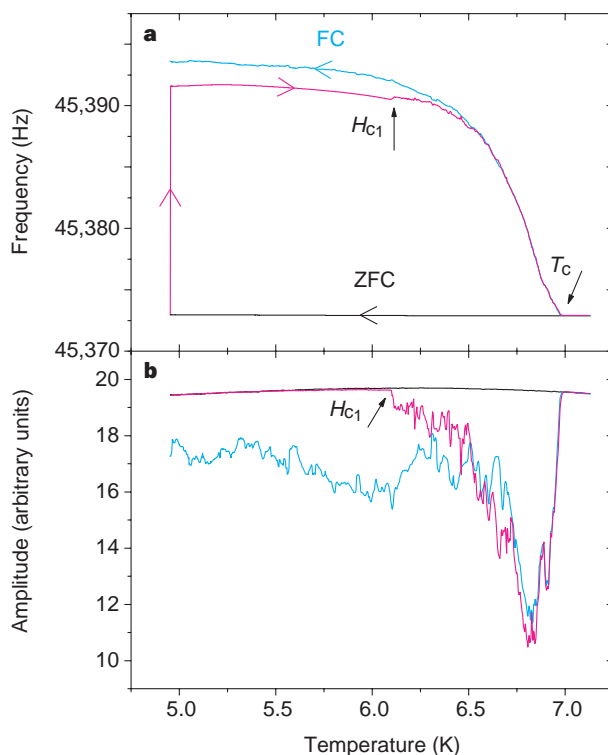


**Figure 2** Temperature dependence of the oscillator resonant frequency (**a**) and amplitude (**b**) for a typical zero-field-cooling/field-cooling (FC) experiment. First the system is cooled, in the absence of a magnetic field, to  $T = 5$  K and the 'background' frequency and amplitude are recorded, shown in the figure by the black lines. Then a magnetic field  $H = 60$  Oe is applied and the temperature is increased to 7.5 K, as shown by the red line. Three different regimes are seen upon heating: (1) the Meissner regime, where shielding currents flow on the surface of the superconductor, yielding an increase in the resonance frequency and no change in amplitude; (2) the lower critical field  $H_{c1}(T)$  for flux-line penetration, at which the motion of flux lines inside the superconductor causes dissipation and decreases the oscillation amplitude; (3) the critical temperature, at which both the frequency and the amplitude merge with the background signal. The blue line shows the field-cooling process. Here flux lines form in the superconductor below the critical temperature. The shape of the frequency changes is given by many factors, including the number of flux lines and the pinning strength, giving rise to a complex structure in the oscillator frequency and amplitude.

behaviour with increasing field is the mesoscopic nature of our system. As the vortices enter the sample, sometimes the entire ensemble is better pinned and the frequency increases but sometimes, because of interactions, it is less well pinned and the frequency decreases. The lower trace is  $B(H)$  extracted from the data by counting vortices. In this case, for  $N(H)$  flux lines in

the sample and a sample cross-section area  $S = 22 \times 1.6 \mu\text{m}^2$ , we have  $B \approx N(H)\Phi_0/S$ .

Figure 3c shows a field sweep at a temperature of 6.8 K for both a ramp up (red line) after a ZFC and a ramp down (blue line). Clearly three regimes can be distinguished. Below  $H_{c1}$  at  $\sim 12.5$  Oe, the Meissner response is reversible. Above  $H_{c1}$  between 12.5 and  $\sim 30$  Oe, the response is irreversible. This is the region where the vortex–vortex interactions are weak enough for the response to depend on field history. Above  $\sim 30$  Oe, one sees a reversible regime in which the response does not depend on field history. In this regime the vortex interactions are strong enough for the ensemble to appear always to find its minimum energy configuration. Note that this regime is still mesoscopic in the sense that the response is highly structured and not monotonic with field. There are  $\sim 20$  flux lines in this part of the curve; the detailed pinning landscape influences how the effective magnetic moment fluctuates with increasing field. This plot is thus a ‘fingerprint’ of the disorder in this specific sample. Taken together, Figs 2 and 3 provide evidence of the mesoscopic (ref. 9) behaviour of a small number of vortices in a finite-sized sample in which the details of the pinning sites produces sample-specific structure in the magnetization of the superconductor.

To describe our results theoretically we determine the constitutive relation  $B(H)$  for a low-temperature vortex array interacting strongly with point disorder. We first note that both the in-plane and out-of-plane London penetration depths  $\lambda_{\perp}(0) = 69$  nm and  $\lambda_c(0) = 230$  nm are comparable to the  $d = 1.6 \mu\text{m}$   $c$ -axis sample dimension at the elevated temperatures  $T/T_c = 0.95$  of interest here<sup>10</sup>. Provided that a vortex feels the confining effect of the surfaces perpendicular to the  $c$  axis many times, we can model flux penetration by a collection of confined ‘1 + 1’-dimensional vortex lines stretched out in the field direction  $y$  (with dimension  $L = 49 \mu\text{m}$ ) wandering transversely in the  $x$  direction (with dimension  $W = 22 \mu\text{m}$ ) and interacting with a random point-like pinning potential. Consider first a single vortex line with trajectory  $x(y)$ . Adapting the treatment for 2 + 1-dimensional vortices in refs. 11 and 12, we assume that this trajectory occurs with probability proportional to  $\exp[-E/T]$  with an energy

$$E = \int_0^L dy \left\{ \frac{1}{2} g [dx(y)/dy]^2 + V[x(y), y] \right\}$$

where  $g = \phi_0^2/16\pi^2\lambda_{\perp}(T)\lambda_c(T)$  is the vortex tilt modulus in the  $x$  direction,  $\phi_0$  the flux quantum and  $V(x, y)$  a coarse-grained random pinning potential with disorder average  $\overline{V(x, y)V(x', y')} \approx \Delta\delta_{\xi_{\perp}}(x - x')\delta(y - y')$ . Here,  $\delta_{\xi_{\perp}}(x)$  is a delta function smeared on the scale of the in-plane coherence length  $\xi_{\perp}$ , and  $\Delta$  is the effective disorder strength. As pointed out by Huse *et al.*<sup>13</sup> the associated free energy obeys a noisy Burgers equation that can be solved exactly<sup>14</sup>. Although an extensive theoretical literature<sup>15</sup> surrounds this model, our experiment seems to be one of the first to probe this important problem in 1 + 1-dimensional statistical mechanics directly. A key prediction<sup>13–15</sup> for a vortex trajectory pinned by point disorder reads

$$\langle \Delta x^2(l) \rangle \equiv \langle |x(y+l) - x(y)|^2 \rangle \approx \xi_{\perp}^2 (ll_c)^{2\zeta}$$

where  $\xi_{\perp}(0) = 77 \text{ \AA}$ , the angular brackets represent a thermal average and  $l_{\perp} = \xi_{\perp}(g^2\xi_{\perp}^2/\Delta)$  (we assume  $\xi_{\perp} > l_c$ ). On scales larger than  $l_c$ , vortices are strongly pinned with anomalous wandering exponent  $\zeta = 2/3$ . The pinning energy associated with a vortex segment of length  $l > l_c$  also grows with  $l$ ,  $U_p(l) \approx g\xi_{\perp}(ll_c)^{2\zeta-1}$ . We neglect, throughout, dimensionless constants of order unity. Different results apply for  $T > T^*$ , where  $T^*$  is determined self-consistently from  $T^* = (\Delta g(T^*)\xi_{\perp}(T^*))^{1/3}$ . For  $T^* < T < T_c$ , one finds different scale factors,  $\langle \Delta x^2(l) \rangle = (Tl_c/g)(ll_c)^{2\zeta}$  and  $U_p(l) = T(ll_c)^{2\zeta-1}$  with  $l_c(T) = T^3/g\Delta$ . For  $\text{NbSe}_2$ ,  $(T_c - T^*)/T_c \approx 10^{-5}$ , so this regime is not relevant to our experiments.

As more vortices enter the sample, their transverse wandering to optimize the pinning potential is limited by collisions with their

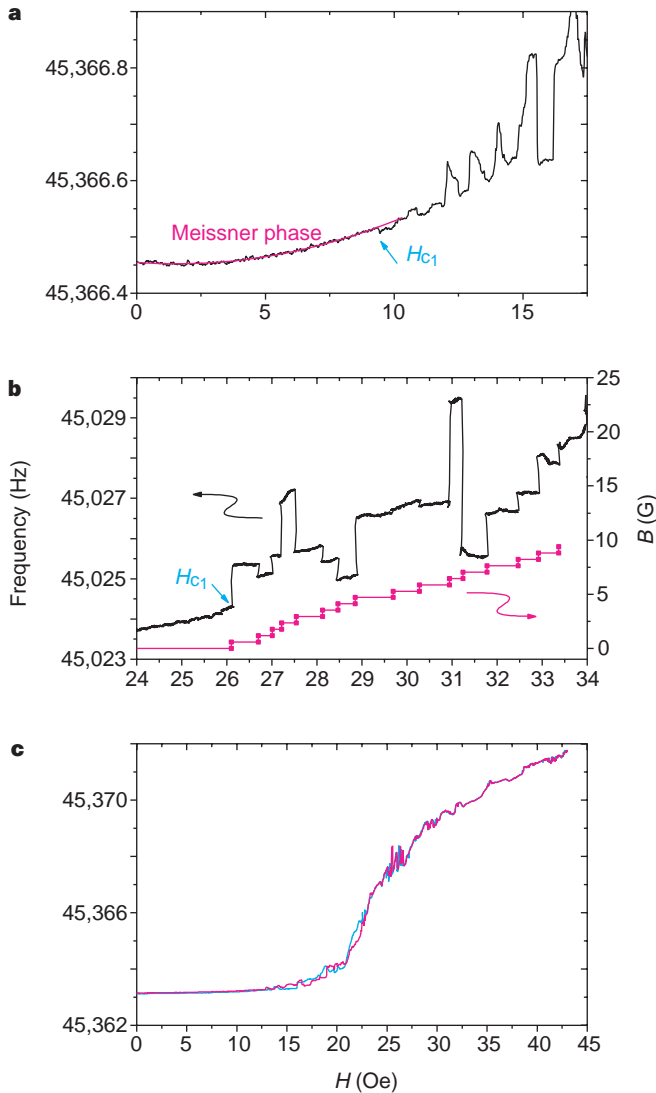


**Figure 3** Three different field dependences of the resonant frequency at the fixed temperatures, 6.9 K (**a**), 6.65 K (**b**) and 6.8 K (**c**). **a**, Below  $H_{c1} = 9$  Oe we see the  $H^2$  dependence of the frequency shift owing to the Meissner state, highlighted by a polynomial fit in red. Above  $H_{c1}$  a series of peaks reflect the penetration of individual flux lines as the field is increased. **b**, the magnetic field was cycled up and down at each point in steps of 0.1 Oe to reveal local irreversibilities. The region below  $H = 26$  Oe, corresponding to the Meissner shielding currents, is reversible as expected. Above  $H_{c1}$  we obtain reversible mesas separated by irreversible jumps. Each jump is associated with a single flux line entering the sample. The lower trace is  $B(H)$  extracted from the data by counting vortices. Note the linear dependence near  $H_{c1}$ . **c**, A large-scale field sweep at a fixed temperature. The red line shows the frequency shift as the field is increased, the blue line as it is decreased. Three regions can be distinguished: at low fields, there is a Meissner phase with the expected  $H^2$  change in frequency; above  $H_{c1}$  we see an irreversible regime that changes into a reversible one at  $H = 30$  Oe. The structure of the resonant frequency above  $H = 30$  Oe is given by the number of flux lines, the shape of the sample, the structure of the flux line lattice and the pinning landscape. In this regime the flux line lattice relaxes to exactly the same structure regardless of the previous field history for our field sweep rate of  $0.02 \text{ Oe s}^{-1}$ .

neighbours when  $\langle \Delta x^2(l^*) \rangle = a_0^2$ , where  $a_0$  is the vortex spacing. The effective value of  $l$  that enters  $U_p(l)$  is thus  $l^* = l_c(a_0/\xi_\perp)^{1/\zeta} \propto B^{-3/2}$ , where  $B = \phi_0/da_0$  is the field associated with a planar array of vortices. On balancing the energy gain per unit area above  $H_{c1}$  of  $N = W/a_0$  wandering flux lines,  $g(H - H_{c1})/H_{c1}a_0 \equiv gha_0$ , against the pinning energy density  $U(l^*)/l^*a_0$  lost because of collisions between lines, we find the constitutive relation

$$B = (\phi_0/\xi_\perp d)(l_c h/\xi_\perp)^{\zeta/2(1-\zeta)} \equiv \frac{g^2 \xi_\perp \phi_0}{d\Delta} (H - H_{c1})/H_{c1}$$

for  $\zeta = 2/3$ , which is consistent with work on related problems<sup>16,17</sup> with point disorder in 1 + 1 dimensions. For an analogous power-law constitutive relation in 2 + 1 dimensions, see ref. 12. To test our result we have extracted  $B(H)$  from the data in Fig. 3b and plotted it as the 'staircase' in that figure. The data are a discrete approximation to the continuum prediction of a linear  $B(H)$  near  $H_{c1}$ , thus confirming the anomalous wandering exponent  $\zeta = 2/3$ . This result is in striking contrast to the vertical slope predicted by Abrikosov's original theory of perfectly straight vortices in clean samples with exponential repulsion. From the slope of this linear dependence we obtain a simple measure of  $\Delta$  and confirm that  $\xi_\perp > l_c$ .

Qualitative arguments based on this simple model suggest that relaxation times decrease markedly as the number of collisions grows with increasing  $B$ , leading to reversible behaviour for large  $B$  with residual fluctuations  $\sqrt{\langle \delta B^2 \rangle} \propto B^{-1/4}$ . We expect that fluctuations in this regime provide a 'fingerprint' of the disorder in the sample. Universal sample-to-sample fluctuations have in fact been predicted for large planar assemblies of vortex lines strongly pinned by point disorder<sup>18,19</sup>.

The study of the 1 + 1-dimensional random potential has been an important starting point in theoretical statistical physics and its investigation of disorder-dominated systems. This experiment is the first that directly studies this famous problem. We believe that the study of mesoscopic vortex physics might become an important new area of research for condensed-matter scientists. □

Received 2 December 1998; accepted 26 February 1999.

- Safar, H. *et al.* Experimental evidence for a 1st-order vortex-lattice-melting transition in untwinned single-crystal  $\text{YBa}_2\text{Cu}_3\text{O}_7$ . *Phys. Rev. Lett.* **69**, 824–827 (1992).
- Brézin, E., Nelson, D. R. & Thiaville, A. Fluctuation effects near  $H_{c2}$  in type-II superconductors. *Phys. Rev. B* **31**, 7124–7132 (1985).
- Kleiman, R. N., Agnolet, G. & Bishop, D. J. Two-level systems observed in the mechanical properties of single-crystal silicon at low temperatures. *Phys. Rev. Lett.* **59**, 2079–2082 (1987).
- Kleiman, R. N., Kaminsky, G. K., Reppy, J. D., Pindak, R. & Bishop, D. J. Single-crystal silicon high-Q torsional oscillators. *Rev. Sci. Instrum.* **56**, 2088–2091 (1985).
- Bishop, D. J. & Reppy, J. D. Study of the superfluid transition in two-dimensional  $^4\text{He}$  films. *Phys. Rev. Lett.* **40**, 1727–1730 (1978).
- Bolle, C. A., de la Cruz, F., Gammel, P. L., Waszczak, J. V. & Bishop, D. J. Observation of tilt induced orientational order in the magnetic flux lattice in 2H-NbSe<sub>2</sub>. *Phys. Rev. Lett.* **71**, 4039–4042 (1993).
- Duarte, A. *et al.* Dynamically induced disorder in the vortex lattice of 2H-NbSe<sub>2</sub>. *Phys. Rev. B* **53**, 11336–11339 (1996).
- Yaron, U. *et al.* Neutron diffraction studies of flowing and pinned magnetic flux lattices in 2H-NbSe<sub>2</sub>. *Phys. Rev. Lett.* **73**, 2748–2751 (1994).
- Akkermans, E., Montambaux, Pichard, J. I. & Zinn-Justin, J. (eds) *Mesoscopic Quantum Physics* (North-Holland, Amsterdam, 1994).
- de Trey, P., Gygax, S. & Jan, J.-P. Anisotropy of the Ginzburg–Landau parameter  $\kappa$  in NbSe<sub>2</sub>. *J. Low Temp. Phys.* **11**, 421–434 (1973).
- Nelson, D. R. Vortex entanglement in high- $T_c$  superconductors. *Phys. Rev. Lett.* **60**, 1973–1976 (1988).
- Natterman, T. & Lipowsky, R. Comment on vortex entanglement in high- $T_c$  superconductors. *Phys. Rev. Lett.* **61**, 2508 (1988).
- Huse, D. A., Henley, C. L. & Fisher, D. S. Response on comment on roughening by impurities at finite temperature. *Phys. Rev. Lett.* **55**, 2924 (1985).
- Forster, D., Nelson, D. R. & Stephen, M. J. Large-distance and long-time properties of a randomly stirred fluid. *Phys. Rev. A* **16**, 732–749 (1977).
- Halpin-Healy, T. & Zhang, Y. Kinetic roughening phenomena, stochastic growth, directed polymers and all that. *Phys. Rep.* **254**, 215–415 (1995).
- Hwa, T., Nelson, D. R. & Vinokur, V. M. Flux-line pinning by competing disorders. *Phys. Rev. B* **48**, 1167–1174 (1993).
- Hwa, T. & Lässig, M. Similarity detection and localization. *Phys. Rev. Lett.* **76**, 2591–2594 (1996).
- Hwa, T. & Fisher, D. S. Vortex glass phase and universal susceptibility variations in planar arrays of flux lines. *Phys. Rev. Lett.* **72**, 2466–2469 (1994).
- Fisher, M. P. A. Vortex-glass superconductivity: a possible new phase in bulk high- $T_c$  oxides. *Phys. Rev. Lett.* **62**, 1415–1418 (1989).

**Acknowledgements.** We thank J. Blatter, T. Hwa, V. Kogan and V. Vinokur for helpful discussions.

Correspondence and requests for materials should be addressed to D.J.B. (e-mail: djb@lucent.com).

## Influence of a knot on the strength of a polymer strand

A. Marco Saitta\*, Paul D. Soper†, E. Wasserman† & Michael L. Klein\*

\* Center for Molecular Modeling, Department of Chemistry, University of Pennsylvania, Philadelphia, Pennsylvania 19104-6202, USA

† DuPont Central Research and Development, Expt. Station, Wilmington, Delaware 19880-0328, USA

Many experiments have been done to determine the relative strengths of different knots, and these show that the break in a knotted rope almost invariably occurs at the point just outside the 'entrance' to the knot. The influence of knots on the properties of polymers has become of great interest, in part because of their effect on mechanical properties<sup>2</sup>. Knot theory<sup>3,4</sup> applied to the topology of macromolecules<sup>5–8</sup> indicates that the simple trefoil or 'overhand' knot is likely to be present in any long polymer strand<sup>9–12</sup>. Fragments of DNA have been observed to contain such knots in experiments<sup>13,14</sup> and computer simulations<sup>15</sup>. Here we use *ab initio* computational methods<sup>16</sup> to investigate the effect of a trefoil knot on the breaking strength of a polymer strand. We find that the knot weakens the strand significantly, and that, like a knotted rope, it breaks under tension at the entrance to the knot.

Little is known about the structure and properties of knots at the atomic level. For example, the minimum number of carbon atoms that can be sustained as a trefoil in a polyethylene strand is not well established<sup>5,19</sup>. Polyethylene is the simplest polymer and therefore an excellent generic system to study the fundamental properties of a knotted chain. (Rigorously, a knot is a closed loop; but here, as in ref. 1, we apply the term to a strand with unlinked ends.) As a representative polyethylene-like system we chose the linear molecule *n*-decane (C<sub>10</sub>H<sub>22</sub>). Empirical models that utilize force constants for bond strength, bend and torsion<sup>18–20</sup>, although useful for studying bulk properties of chain molecules, are not applicable to the case of chain rupture. First-principles calculations<sup>16</sup>, on the other hand, have been shown to yield satisfactory results for structural and mechanical properties of hydrocarbon-based polymeric systems<sup>21,22</sup>. The *ab initio* equilibrium structural parameters for such alkanes, after optimization, are in excellent agreement with experiment, with errors in bond lengths and angles smaller than 1%

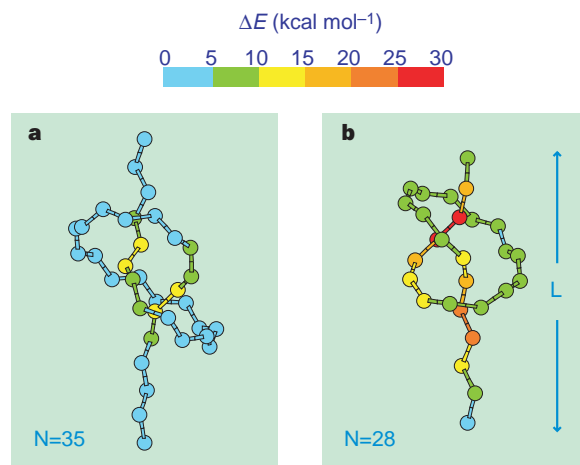


**Figure 1** Strain energy distribution in a knotted polymer strand. Shown are distributions in chains of 35 (a) and 28 (b) carbon atoms taken from constrained classical MD simulations. When the knot is sufficiently tightened, the strain energy localizes most on the bonds immediately outside its entrance points.